CHEMISTRY
A EUROPEAN JOURNAL

DOI: 10.1002/chem.200800602

HP-$Ca_2Si_5N_8$—A New High-Pressure Nitridosilicate: Synthesis, Structure, Luminescence, and DFT Calculations

S. Rebecca Römer,[a] Cordula Braun,[a] Oliver Oeckler,[a] Peter J. Schmidt,[b] Peter Kroll,[c] and Wolfgang Schnick*[a]

Abstract: HP-$Ca_2Si_5N_8$ was obtained by means of high-pressure high-temperature synthesis utilizing the multianvil technique (6 to 12 GPa, 900 to 1200 °C) starting from the ambient-pressure phase $Ca_2Si_5N_8$. HP-$Ca_2Si_5N_8$ crystallizes in the orthorhombic crystal system (*Pbca* (no. 61), $a = 1058.4(2)$, $b = 965.2(2)$, $c = 1366.3(3)$ pm, $V = 1395.7(7) \times 10^6$ pm^3, $Z = 8$, $R1 = 0.1191$). The HP-$Ca_2Si_5N_8$ structure is built up by a three-dimensional, highly condensed nitridosilicate framework with $N^{[2]}$ as well as $N^{[3]}$ bridging. Corrugated layers of corner-sharing SiN_4 tetrahedra are interconnected by further SiN_4 units. The Ca^{2+} ions are situated between these layers with coordination numbers 6+1 and 7+1, respectively. HP-$Ca_2Si_5N_8$ as well as hypothetical orthorhombic o-$Ca_2Si_5N_8$ (isostructural to the ambient-pressure modifications of $Sr_2Si_5N_8$ and $Ba_2Si_5N_8$) were studied as high-pressure phases of $Ca_2Si_5N_8$ up to 100 GPa by using density functional calculations. The transition pressure into HP-$Ca_2Si_5N_8$ was calculated to 1.7 GPa, whereas o-$Ca_2Si_5N_8$ will not be adopted as a high-pressure phase. Two different decomposition pathways of $Ca_2Si_5N_8$ (into Ca_3N_2 and Si_3N_4 or into $CaSiN_2$ and Si_3N_4) and their pressure dependence were examined. It was found that a pressure-induced decomposition of $Ca_2Si_5N_8$ into $CaSiN_2$ and Si_3N_4 is preferred and that $Ca_2Si_5N_8$ is no longer thermodynamically stable under pressures exceeding 15 GPa. Luminescence investigations (excitation at 365 nm) of HP-$Ca_2Si_5N_8$:Eu^{2+} reveal a broadband emission peaking at 627 nm (FWHM = 97 nm), similar to the ambient-pressure phase $Ca_2Si_5N_8$:Eu^{2+}.

Keywords: density functional calculations · high-pressure chemistry · luminescence · nitridosilicates · phase transitions

Introduction

Nitridosilicates and oxonitridosilicates (e.g., γ-Si_3N_4,[1,2] SiAlONs,[3] $Sr_2Si_5N_8$,[4] $Eu_2Si_5N_8$[5]) are well known to exhibit interesting physical properties,[6,7] such as good wear resistance, high decomposition temperature, exceptional oxidation stability, luminescence,[8–10] or nonlinear optical behavior.[11] These material properties are of special interest for industrial applications.[1–11]

During the last two decades, an increasing number of dense high-pressure oxosilicates have been synthesized and their material properties characterized.[12,13] The high technological impact of high-pressure silicate phases is illustrated by the discovery of the extraordinary mechanical hardness of stishovite and post-stishovite SiO_2 polymorphs, which crystallize in the rutile and α-PbO_2 structure types, respectively.[14,15] Their extreme hardness seems to justify their rating as the hardest oxides known so far.[14,15]

The material properties of nitrides are often superior to those of the respective oxides. This observation is attributed to the higher covalency of the constituent chemical bonds and the higher degree of cross-linking in nitride structures compared to oxides.[16] The discovery of spinel-type γ-Si_3N_4 triggered broad research efforts targeting new high-pressure nitridosilicate and oxonitridosilicate phases.[1,2]

[a] S. R. Römer, C. Braun, Dr. O. Oeckler, Prof. Dr. W. Schnick
Department Chemie und Biochemie
Lehrstuhl für Anorganische Festkörperchemie
Ludwig-Maximilians-Universität München
Butenandtstrasse 5–13 (D), 81377 München (Germany)
Fax: (+49) 89-2180-77440
E-mail: wolfgang.schnick@uni-muenchen.de

[b] Dr. P. J. Schmidt
Philips Technologie GmbH
Forschungslaboratorien, Solid State Lighting
Weisshausstrasse 2, 52066 Aachen (Germany)

[c] Prof. Dr. P. Kroll
Department of Chemistry and Biochemistry
The University of Texas at Arlington
700 Planetarium Place, Arlington, TX 76019-0065 (USA)

Supporting information for this article is available on the WWW under http://dx.doi.org/10.1002/chem.200800602.

With the characterization of the new high-pressure phase HP-$Ca_2Si_5N_8$, we illustrate that reconstructive phase transitions for ternary high-pressure nitridosilicates are possible. Through density functional calculations we access the $Ca_2Si_5N_8$–HP-$Ca_2Si_5N_8$–$CaSiN_2$/Si_3N_4 phase diagram up to 100 GPa, by considering phase stability under pressure.

Results and Discussion

Synthesis: For the synthesis of $Ca_2Si_5N_8$, a mixture of Ca metal and $Si(NH)_2$ powder was heated in a radio-frequency furnace at 1650 °C under a nitrogen atmosphere [Eq. (1)].[17,18]

$$2\,Ca + 5\,Si(NH)_2 \rightarrow Ca_2Si_5N_8 + 5\,H_2 + N_2 \qquad (1)$$

Starting from the respective ambient-pressure polymorph, the high-pressure phase HP-$Ca_2Si_5N_8$ was synthesized by employing the multianvil press technique. HP-$Ca_2Si_5N_8$ was synthesized at pressures ranging from 6 to 12 GPa and temperatures between 900 and 1200 °C.[19–21] The molar ratio Ca/Si = 2:5 of HP-$Ca_2Si_5N_8$ was confirmed by energy-dispersive X-ray (EDX) measurements, and no oxygen was detected (see the Experimental Section).

Structure determination: Very small single crystals of HP-$Ca_2Si_5N_8$ were obtained by mechanical fragmentation of the sample from the multianvil experiment. Systematic absences suggested the orthorhombic space group *Pbca* (no. 61). The very low scattering intensity rendered the solution and refinement of the structure difficult. The structure could not be solved by conventional direct methods; however, a solution in space group $P2_12_12_1$ was achieved by means of the dual-space approach.[22] The structure turned out to be centrosymmetric and could be transformed into *Pbca*. It was refined with anisotropic displacement parameters for all atoms. The crystallographic data and details of the data collection are listed in Table 1.

All strong reflections of the powder pattern of HP-$Ca_2Si_5N_8$ were indexed on the basis of the unit cell determined from the single crystal. β-Si_3N_4 was present as a minor impurity. Rietveld refinement was carried out, starting from the atomic parameters of the single-crystal structure of HP-$Ca_2Si_5N_8$. The observed and calculated X-ray powder diffraction patterns as well as the difference profile of the Rietveld refinement are shown in Figure 1.

Structure description: The HP-$Ca_2Si_5N_8$ structure is built up by a three-dimensional, highly condensed nitridosilicate framework with $N^{[2]}$ and $N^{[3]}$ bridging. Corrugated layers of corner-sharing SiN_4 tetrahedra are interconnected by further SiN_4 units. The Ca^{2+} ions are situated between these layers, with coordination numbers 6+1 and 7+1, respectively. Figure 2 shows the crystal structure of HP-$Ca_2Si_5N_8$ viewed along [010]. Half of the nitrogen atoms connect two Si tetrahedral centers ($N^{[2]}$: N1, N2, N3, N4), whereas the others ($N^{[3]}$: N5, N6, N7, N8) bridge three Si atoms.

Table 1. Crystallographic data for HP-$Ca_2Si_5N_8$.

formula	$Ca_2Si_5N_8$
molar mass [g mol^{-1}]	332.63
crystal system	orthorhombic
space group	*Pbca* (no. 61)
cell parameters [pm]	a = 1058.4(10)
	b = 965.2(4)
	c = 1366.3(10)
cell volume [10^6 pm^3]	1395.7(7)
formula units/cell	8
X-ray density [g cm^{-3}]	3.17
absorption coefficient [mm^{-1}]	2.46
F(000)	1328
crystal size [mm^3]	0.12 × 0.08 × 0.04
diffractometer	Stoe IPDS
radiation, monochromator	$Mo_{K\alpha}$ (λ = 71.073 pm), graphite
temperature [K]	293
2θ range [°]	6.0–50
total no. of reflections	5883
independent reflections	1063
observed reflections	505
absorption correction	semiempirical
refined parameters	137
GOF	0.814
R values [$I > 2\sigma(I)$]	$R1$ = 0.0555, $wR2$ = 0.1153
all data	$R1$ = 0.1191, $wR2$ = 0.1377
max./min. residual electron density [e Å^{-3}]	0.521/−0.698

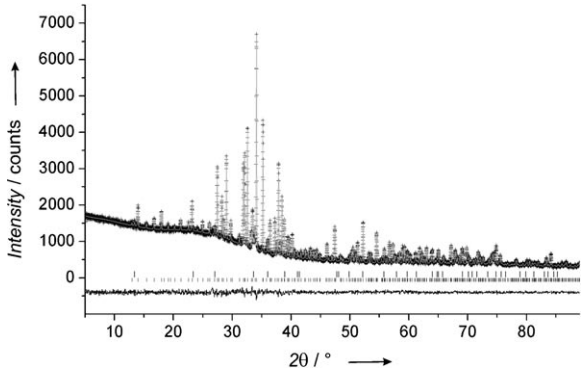

Figure 1. Observed (+) and calculated (——) X-ray powder diffraction patterns and the difference profile of the Rietveld refinement of HP-$Ca_2Si_5N_8$ (λ = 154.06 pm).

The characteristically corrugated layers of the high-pressure phase extend perpendicular to [001], and consist of highly condensed "*dreier*" rings.[23] Within these layers all Si atoms are solely connected by $N^{[3]}$ atoms (see Figure 3). Similar layers of *dreier* rings also exist in $M_2Si_5N_8$ (M = Ca, Sr, Ba),[4,18] but the configuration pattern of the SiN_4 tetrahedra within these layers and the pattern generated by vertices pointing up and down is different for monoclinic $Ca_2Si_5N_8$ and $M_2Si_5N_8$ (M = Sr, Ba). In HP-$Ca_2Si_5N_8$, between zigzag lines (along [010]) with vertices pointing either up or down, another zigzag line is inserted with pairs of tetrahedra vertices pointing alternately up and down (see

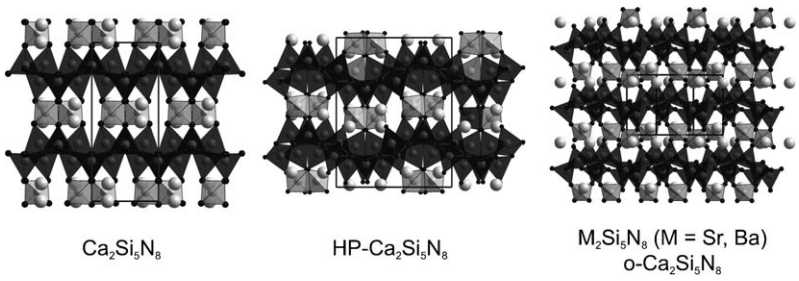

Figure 2. Structures of $Ca_2Si_5N_8$ (view along [001]), HP-$Ca_2Si_5N_8$ (view along [010]), and $M_2Si_5N_8$ (M = Sr, Ba)/o-$Ca_2Si_5N_8$ (view along [¾ 0 ¼]). Ca: light gray, Si: gray, N: black). Layers are highlighted by dark tetrahedra; interconnecting tetrahedra are light gray.

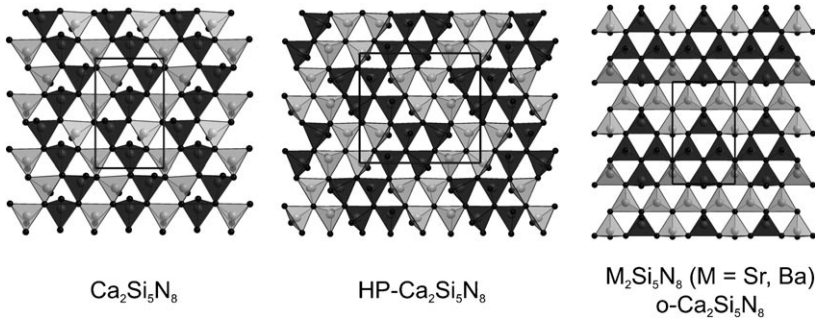

Figure 3. Layers in $Ca_2Si_5N_8$, HP-$Ca_2Si_5N_8$, and $M_2Si_5N_8$ (M = Sr, Ba)/o-$Ca_2Si_5N_8$. Tetrahedra with vertices up: black; tetrahedra with vertices down: light gray.

Figure 3). The cycle-class sequence (i.e., the relative frequency of the Si_nN_n-ring sizes occurring in the network for $n = 1, 2, 3\ldots$) for HP-$Ca_2Si_5N_8$ has been calculated with the program TOPOLAN.[24–27] A comparison to the cycle-class sequence of monoclinic $Ca_2Si_5N_8$ and $M_2Si_5N_8$ (M = Sr, Ba) is given in Table 2. For a detailed discussion, see the next section.

Table 2. Cycle-class sequence[24–27] of $Ca_2Si_5N_8$, o-$Ca_2Si_5N_8$, and HP-$Ca_2Si_5N_8$.

Si_nN_n rings	$n=3$	4	5	6	7	8	9	10
$Ca_2Si_5N_8$	12	4	32	40	166	438	1604	5020
o-$Ca_2Si_5N_8$	10	6	32	50	180	478	1708	5284
HP-$Ca_2Si_5N_8$	39	23	126	191	693	1852	6130	19023

The Si–N bond lengths in HP-$Ca_2Si_5N_8$ are in a typical range of 167–173 pm for $N^{[2]}$ ($Ca_2Si_5N_8$ 167–171 pm,[18] $Sr_2Si_5N_8$ 165–169 pm,[4] $Ba_2Si_5N_8$ 166–171 pm[4]) and 174–180 pm for $N^{[3]}$ ($Ca_2Si_5N_8$ 173–180 pm,[18] $Sr_2Si_5N_8$ 174–179 pm,[4] $Ba_2Si_5N_8$ 174–179 pm[4]). The angles Si-$N^{[2]}$-Si range from 119 to 140° and correspond well with those of previously published nitridosilicates ($Ca_2Si_5N_8$ 116–132°,[18] $Sr_2Si_5N_8$ 125–142°,[4] $Ba_2Si_5N_8$ 128–148°[4]). The same holds true for the Si-$N^{[3]}$-Si angles (HP-$Ca_2Si_5N_8$ 107–128°, $Ca_2Si_5N_8$ 107–127°,[18] $Sr_2Si_5N_8$ 107–127°,[4] $Ba_2Si_5N_8$ 108–128°[4]). The sums of the bond angles Si-$N^{[3]}$-Si for each $N^{[3]}$ adopt values of 344–355°, which are in accordance with those found in other $M_2Si_5N_8$ (M = Ca, Sr, Ba) structures ($Ca_2Si_5N_8$: 352–360°,[18] $Sr_2Si_5N_8$: 341–360°,[4] $Ba_2Si_5N_8$: 344–360°[4]), which indicates nearly planar units $N^{[3]}(SiN_3)_3$.[4,18] The Ca^{2+} ions are 6+1 and 7+1 coordinated by nitrogen atoms in distances of 241–330 pm (ambient-pressure $Ca_2Si_5N_8$ (CN(Ca) = 7): 232–313 pm). The coordination is described as 6+1 and 7+1 rather than 7 and 8, due to the small contribution of the last nitrogen atoms to the effective coordination number, as calculated by the program MAPLE.[28–30]

The calculation of bond-valence sums for HP-$Ca_2Si_5N_8$ with the help of bond length/bond strength[31,32] (ΣV) and Chardi[33] (ΣQ) yielded the expected formal ionic charges of the atoms (Ca +1.96 to +1.99, Si +3.93 to +4.12, N −2.87 to −3.18). As expected, the Madelung part of the lattice energy (MAPLE)[28–30] of HP-$Ca_2Si_5N_8$ is almost identical to the sum of the respective MAPLE values of the components $CaSiN_2$ and β-Si_3N_4 (see Table 3).

Table 3. MAPLE values for HP-$Ca_2Si_5N_8$ [kJ mol^{-1}].

Compound	$Ca_2Si_5N_8$	HP-$Ca_2Si_5N_8$	$CaSiN_2$	β-Si_3N_4
MAPLE	98561	98536	22633	53226

	MAPLE	Difference	Difference [%]
2 $CaSiN_2$ + β-Si_3N_4	23524		
$Ca_2Si_5N_8$	23541	17	0.07
HP-$Ca_2Si_5N_8$	23535	10	0.04

Atom[a]	$Ca1^{2+}$	$Ca2^{2+}$	$Si3^{4+}$	$Si4^{4+}$	$Si5^{4+}$	$Si6^{4+}$	$Si7^{4+}$
MAPLE	2078	2029	9596	9653	9671	9607	10190

Atom[a]	$N1^{3-}$	$N2^{3-}$	$N3^{3-}$	$N4^{3-}$	$N5^{3-}$	$N6^{3-}$	$N7^{3-}$	$N8^{3-}$
MAPLE	5347	5481	5448	5354	5962	5977	6078	6049

total MAPLE (HP-$Ca_2Si_5N_8$) exp.	98514
total MAPLE (2× $CaSiN_2$ + β-Si_3N_4) theor.	98531
difference Δ [%]	0.01

[a] Typical partial MAPLE values [kJ mol^{-1}]: Ca^{2+}: 1900–2100, Si^{4+}: 9000–10200, $N^{[2]3-}$: 4000–6000, $N^{[3]3-}$: 5200–6300.

Comparison to $Ca_2Si_5N_8$ and $M_2Si_5N_8$ (M=Sr, Ba): HP-$Ca_2Si_5N_8$ exhibits rather similar structural features to monoclinic $Ca_2Si_5N_8$ and $M_2Si_5N_8$ (M = Sr, Ba). The ambient-pressure phase of $Ca_2Si_5N_8$[18] crystallizes in the monoclinic non-centrosymmetric space group *Cc* (no. 9) and HP-$Ca_2Si_5N_8$ in the orthorhombic centrosymmetric space group *Pbca* (no. 61). $Sr_2Si_5N_8$ and likewise isotypic $Ba_2Si_5N_8$ crystallize in

the orthorhombic noncentrosymmetric space group $Pmn2_1$ (no. 31).[4] The three structures share common basic structural motifs. They are built up by layers of corner-sharing SiN_4 tetrahedra comprising *dreier* rings. These layers are interconnected by further SiN_4 units to form a three-dimensional network. The M^{2+} ions are situated between these layers and are predominantly coordinated by $N^{[2]}$.

The SiN_4 tetrahedra in the layers of all three structures have three $N^{[3]}$ and one $N^{[2]}$, where the $N^{[3]}$ exclusively form the intralayer bonds, whereas the $N^{[2]}$ are situated on the vertices pointing either up or down. The molar fraction of tetrahedra pointing up and down is equal according to the formula $[(Si^{[4]})_5(N^{[2]})_4(N^{[3]})_4]^{4-}$ of the nitridosilicate network. The layers in the three $M_2Si_5N_8$ structures differ in their degree of corrugation and the pattern of tetrahedra pointing up and down. Although the layers are strongly corrugated in $M_2Si_5N_8$ (M = Sr, Ba) and HP-$Ca_2Si_5N_8$, they are significantly less corrugated in monoclinic $Ca_2Si_5N_8$ (see Figure 2).

The known $M_2Si_5N_8$ structures are related to that of the mineral sinoite, Si_2N_2O.[34] Sinoite contains the same honeycomb layers, even though none of the $M_2Si_5N_8$ layers exhibits the same up–down pattern as the layers in sinoite. The vertices of tetrahedra pointing up and down in Si_2N_2O are occupied by O atoms, which connect two layers. For $M_2Si_5N_8$ the bridging O atoms are substituted by SiN_4 tetrahedra, which results in a three-dimensional charged network: ${}^3_\infty[[Si^{[4]}N^{[3]}]_4[Si^{[4]}N_4^{[2]}]]^{4-}$.

The layers in monoclinic $Ca_2Si_5N_8$ exhibit a rather simple pattern of alternating zigzag lines of tetrahedra (along [001]) with their vertices pointing either up or down, whereas the pattern becomes more complex for HP-$Ca_2Si_5N_8$. The up and down pattern in $M_2Si_5N_8$ (M = Sr, Ba) is not related to the pattern of either $Ca_2Si_5N_8$ structure, but exhibits groups of four tetrahedra with their vertices pointing in the same direction. These groups are arranged in "corner-sharing" rows along [100] (see Figure 3).

HP-$Ca_2Si_5N_8$ can be described as a centrosymmetric variant of the noncentrosymmetric ambient-pressure modification. From Figure 2 it is evident that the application of pressure formally shifts two single unit cells of $Ca_2Si_5N_8$ towards each other. This introduces a center of inversion which doubles the unit cell of HP-$Ca_2Si_5N_8$ compared to its ambient-pressure phase and still allows for the extreme corrugation of the SiN_4 tetrahedra layers. Despite the similarity between monoclinic $Ca_2Si_5N_8$ and HP-$Ca_2Si_5N_8$, the phase transformation is reconstructive, as required for transforming the differently patterned layers. Therefore, the activation energy for the retransformation into the ambient-pressure phase is high enough to render HP-$Ca_2Si_5N_8$ metastable. Monoclinic noncentrosymmetric $Ca_2Si_5N_8$ exhibits nonlinear optical behavior,[11] whereas HP-$Ca_2Si_5N_8$ unequivocally crystallizes with a center of inversion. Furthermore, the Raman spectra of both monoclinic $Ca_2Si_5N_8$ and HP-$Ca_2Si_5N_8$ are different (for further details on the Raman spectra, see Figures S1 and S2 in the Supporting Information).

For all three structures, monoclinic $Ca_2Si_5N_8$, HP-$Ca_2Si_5N_8$, and $M_2Si_5N_8$ (M = Sr, Ba), the coordination numbers of the M^{2+} ions were determined by calculating effective coordination number (ECoN)[28] values with MAPLE[29,30] and searching for gaps in the M^{2+}–N distance distributions. For $Ca_2Si_5N_8$ the coordination number 7 was derived for both crystallographically independent Ca^{2+} ions, whereas in HP-$Ca_2Si_5N_8$ one Ca^{2+} ion is 6+1 coordinated and the other exhibits 7+1 coordination. This results in an increased coordination number for half of the Ca atoms. For both $Sr_2Si_5N_8$ and $Ba_2Si_5N_8$ a coordination number of 10 was derived for both M^{2+} ions (see Figure 4).

Luminescence: To study photoluminescence, samples of HP-$Ca_2Si_5N_8$ were doped with 1 mol% Eu^{2+}. Under daylight HP-$Ca_2Si_5N_8$:Eu^{2+} exhibits a light orange body color due to $4f^7(^8S_{7/2}) \rightarrow 4f^65d$ absorption of Eu^{2+} in the blue to green spectral range. Figure 5 shows the excitation and emission spectra of several samples of HP-$Ca_2Si_5N_8$:Eu^{2+}. The luminescence spectra exhibit a broadband emission peaking at

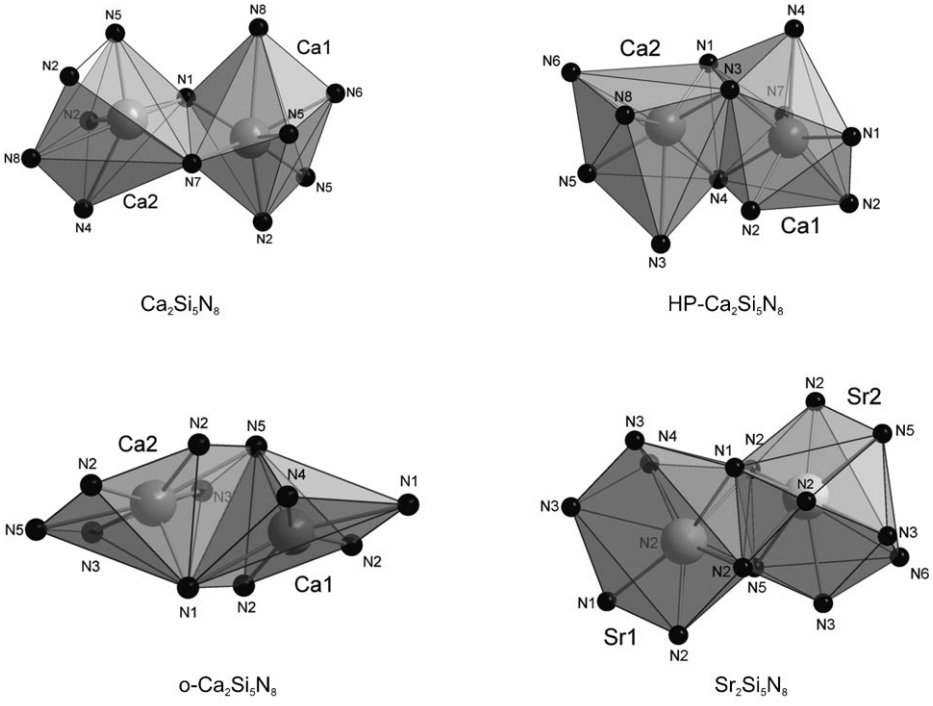

Figure 4. CaN_x polyhedra in $Ca_2Si_5N_8$, HP-$Ca_2Si_5N_8$, o-$Ca_2Si_5N_8$, and $Sr_2Si_5N_8$.

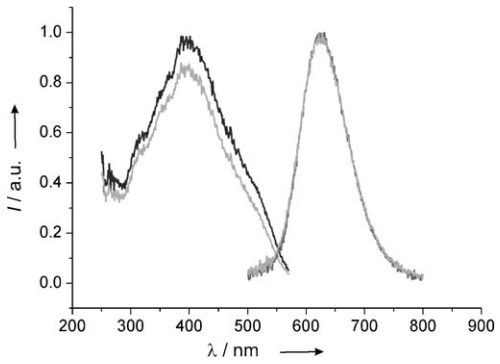

Figure 5. Excitation (black, $\lambda_{exc}=390$ nm) and emission (gray, $\lambda_{mon}=627$ nm) spectra of different samples of HP-$Ca_2Si_5N_8$:Eu^{2+}. *I*: intensity.

627 nm, typical for Eu^{2+} in a nitridosilicate network, which resembles that reported for $Sr_2Si_5N_8$:Eu^{2+}.[11] No Eu^{3+} emission line spectrum was detected by UV excitation at 365 nm. A comparison of the emission spectra of $Ca_2Si_5N_8$:Eu^{2+} and HP-$Ca_2Si_5N_8$:Eu^{2+} in Figure 6 shows that the high-pressure

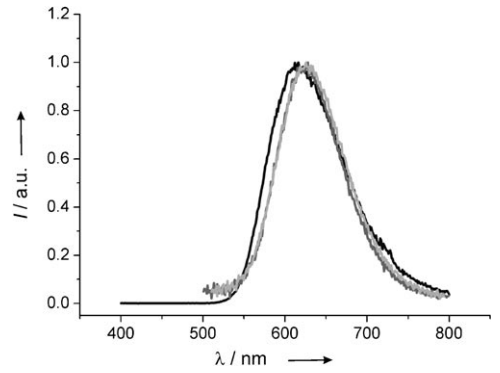

Figure 6. Comparison of the emission spectra of $Ca_2Si_5N_8$:Eu^{2+} (black, $\lambda_{mon}=616$ nm) and HP-$Ca_2Si_5N_8$:Eu^{2+} (gray, light gray, $\lambda_{mon}=627$ nm).

phase has a narrower emission band (full width at half maximum, FWHM = 97 nm) compared to the monoclinic ambient-pressure phase (FWHM = 111 nm). In both phases, that is, HP-$Ca_2Si_5N_8$:Eu^{2+} and ambient-pressure $Ca_2Si_5N_8$:Eu^{2+}, comparable Stokes shifts are observed. Thus, differences in emission bandwidths can be explained by different chemical differentiation of the cation sites in the ambient and high-pressure phases, respectively. Its spectroscopic properties render the HP-$Ca_2Si_5N_8$:Eu^{2+} phase as a promising phosphor for warm white-light light-emitting diode applications.[8,35–37]

DFT calculations: Two structures were considered as possible high-pressure phases for $Ca_2Si_5N_8$: 1) the structure of the experimentally found HP-$Ca_2Si_5N_8$ and 2) that of hypothetical orthorhombic o-$Ca_2Si_5N_8$, which is isostructural to the ambient-pressure modifications of $Sr_2Si_5N_8$ and $Ba_2Si_5N_8$. We also looked for further high-pressure phases among defective NaCl and CsCl structures as well as filled spinel and Th_3P_4 structures. None of the additional candidates we found will be attainable below 70 GPa, however.

Structure optimization for $Ca_2Si_5N_8$, HP-$Ca_2Si_5N_8$, and o-$Ca_2Si_5N_8$: Structure optimization for monoclinic $Ca_2Si_5N_8$[38] and HP-$Ca_2Si_5N_8$ within the local density approximation (LDA) and general gradient approximation (GGA) shows the trends of slightly under- and overestimating cell parameters and accordingly the cell volumes typical for such compounds. Nevertheless, the calculated unit cell parameters and equilibrium volumes are in good accordance with experimental values. No significant changes in bond lengths or substantial distortions of the structure were observed (for detailed data on bond lengths for any discussed structure, see the Supporting Information). Data on the structure optimizations of $Ca_2Si_5N_8$ and HP-$Ca_2Si_5N_8$ are given in Tables 4 and 5.

Table 4. Structure optimization of $Ca_2Si_5N_8$.

	Experimental[18]	LDA	GGA
space group	*Cc* (no. 9, monoclinic)		
a [pm]	1435.2(3)	1426.7	1442.1
b [pm]	561.0(1)	555.8	563.4
c [pm]	968.9(2)	960.5	974.9
β [°]	112.06(3)	112.033	111.922
V [10^6 pm^3]	723.00	705.98	734.73
V f.u. [10^6 pm^3]	180.75	176.50	183.68
ρ [g cm^{-1}]	3.06	3.13	3.01

Table 5. Structure optimization of HP-$Ca_2Si_5N_8$.

	Experimental	LDA	GGA
space group	*Pbca* (no. 61, orthorhombic)		
a [pm]	1058(2)	1048.3	1065.9
b [pm]	965.2(4)	957.3	970.8
c [pm]	1366(2)	1352.3	1368.2
V [10^6 pm^3]	1395(2)	1357.01	1415.79
V f.u. [10^6 pm^3]	174	169.63	176.97
ρ [g cm^{-1}]	3.17	3.26	3.12

The resulting cell parameters and the obtained equilibrium volumes for the hypothetical o-$Ca_2Si_5N_8$ are given in Table 6. The calculated bond lengths (LDA: Si–N 166–175 pm, Ca–N 235–308 pm; GGA: Si–N 168–178 pm, Ca–N 238–314 pm) are all in the range of those in $Ca_2Si_5N_8$ and HP-$Ca_2Si_5N_8$. As expected, Si–N[2] bonds are shorter than Si–N[3] bonds.

Table 6. Structure optimization of o-$Ca_2Si_5N_8$.

	$Sr_2Si_5N_8$[4]	LDA	GGA
space group	$Pmn2_1$ (no. 31, orthorhombic)		
a [pm]	571.0(2)	562.2	570.4
b [pm]	682.2(2)	665.0	675.3
c [pm]	934.10(2)	926.2	937.9
V [10^6 pm^3]	363.9(2)	346.26	361.24
V f.u. [10^6 pm^3]	182.0	173.13	180.62
ρ [g cm^{-1}]	3.90	3.19	3.06

For all optimized structures the coordination numbers of the M^{2+} ions were determined by calculating ECoN[29] values with MAPLE[29,30] and searching for gaps in the M^{2+}–N distance distributions, to compare them with the data for the experimentally determined structures. For both monoclinic $Ca_2Si_5N_8$ and HP-$Ca_2Si_5N_8$ the same coordination numbers as in the experimentally determined structures were derived. In o-$Ca_2Si_5N_8$, one Ca^{2+} is sixfold coordinated and one is sevenfold coordinated by N, whereas M^{2+} in $M_2Si_5N_8$ (M = Sr, Ba) is tenfold coordinated by N.

The coordinative bond lengths Ca–N ($Ca_2Si_5N_8$: Ca–N(LDA) 228–315 pm; Ca–N(GGA) 232–320 pm; HP-$Ca_2Si_5N_8$ Ca–N(LDA): 237–331 pm; Ca–N(GGA) 240–337 pm; o-$Ca_2Si_5N_8$ see values given above) correspond quite well to the sum of the ionic radii (ionic radii after Shannon:[39] Σ(Ca(VI)–N 246 pm, Σ(Ca(VII)–N 252 pm; ionic radii after Baur:[40] Ca(VI)–N 247–249 pm).

Comparison of the density of the three considered $Ca_2Si_5N_8$ structures shows that the ambient-pressure phase $Ca_2Si_5N_8$ has the lowest value ($\rho = 3.06$ (experimental), 3.13 (LDA), 3.01 g cm^{-1} (GGA)). The next denser structure is o-$Ca_2Si_5N_8$ ($\rho = 3.19$ (LDA), 3.06 g cm^{-1} (GGA)), with HP-$Ca_2Si_5N_8$ being the densest phase ($\rho = 3.17$ (experimental), 3.26 (LDA), 3.12 g cm^{-1} (GGA)). Within the GGA, $Ca_2Si_5N_8$ has the lowest energy (−116.6048 eV per formula unit), followed by HP-$Ca_2Si_5N_8$ (−116.5358 eV) and o-$Ca_2Si_5N_8$ (−116.0932 eV).

***E–V* calculations for high-pressure phase transitions**: For calculating the enthalpy–pressure phase diagram of $Ca_2Si_5N_8$, the GGA is preferred over the LDA, because the latter tends to favor higher coordinated structures and, consequently, fails to reproduce the experimental transition pressures. The GGA performs much better on this behalf.[41] Therefore, all calculated enthalpy differences and transition pressures given in this work are based on GGA calculations.

The energy–volume (*E–V*) curves of our three structures of $Ca_2Si_5N_8$ are depicted in Figure 7, from which the enthalpy was extracted as a function of pressure as illustrated in Figure 8. Accordingly, the transition pressure of monoclinic $Ca_2Si_5N_8$ to HP-$Ca_2Si_5N_8$ was calculated with 1.7 GPa (for details, see Table 7), which reasonably agrees with the experimental value. The phase transformation of $Ca_2Si_5N_8$ into HP-$Ca_2Si_5N_8$ could be observed at 6 GPa and 900 °C. We attribute the difference between the calculated and experimental transition pressure to kinetic effects of the phase transformation.

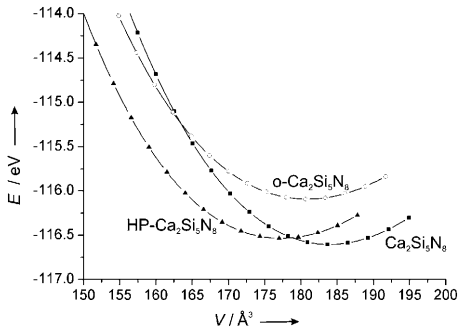

Figure 7. *E–V* diagram for all three considered phases of $Ca_2Si_5N_8$.

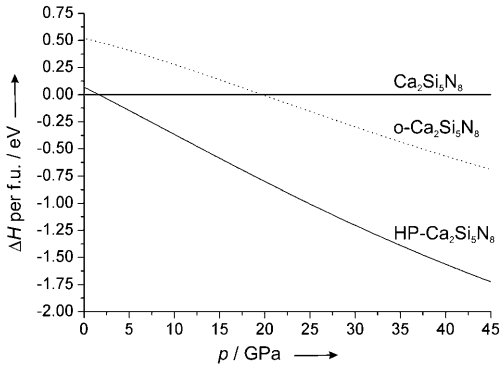

Figure 8. Enthalpy–pressure diagram for the transition of $Ca_2Si_5N_8$ to HP-$Ca_2Si_5N_8$ ($p_t = 1.7$ GPa) and o-$Ca_2Si_5N_8$ ($p_t = 20$ GPa) (Murnaghan equation of state (EOS) evaluation).

Table 7. Transition pressures [GPa] derived from different fitting procedures of *E–V* data for $Ca_2Si_5N_8$ into HP-$Ca_2Si_5N_8$ and o-$Ca_2Si_5N_8$.

	HP-$Ca_2Si_5N_8$	o-$Ca_2Si_5N_8$
spline	1.6	20.2
Murnaghan	1.7	19.9
Birch	1.7	19.9
Vinet	1.7	19.8
Δ_{max}	0.1	0.4

At 20 GPa the enthalpy of o-$Ca_2Si_5N_8$ becomes more favorable than that of monoclinic $Ca_2Si_5N_8$. However, HP-$Ca_2Si_5N_8$ remains the energetically most stable phase, which is in accordance with the experiment (see Figure 8).

Furthermore, calculations of the phonon band structure indicate that o-$Ca_2Si_5N_8$ comprises imaginary vibrational modes within the Brillouin zone already at ambient pressure, amplified at higher pressures. Hence, this particular structure is already dynamically unstable at ambient pressure. Monoclinic and HP-$Ca_2Si_5N_8$ were proven to be free of such imaginary vibrational modes.

Decomposition reactions under pressure: In addition to pressure-induced phase transformations, two possible decomposition pathways under pressure were examined: 1) the decomposition of $Ca_2Si_5N_8$ into the binary nitrides Ca_3N_2 and Si_3N_4 [Eq. (2)] and 2) decomposition into $CaSiN_2$ and Si_3N_4 [Eq. (3)].

$$3\,Ca_2Si_5N_8 \rightarrow 2\,Ca_3N_2 + 5\,Si_3N_4 \quad (2)$$

$$Ca_2Si_5N_8 \rightarrow 2\,CaSiN_2 + Si_3N_4 \quad (3)$$

Structure optimization for Si_3N_4, Ca_3N_2, and $CaSiN_2$: The structures of β-Si_3N_4 and γ-Si_3N_4 were optimized within LDA and GGA. β-Si_3N_4 crystallizes in the hexagonal space

group $P6_3/m$ (no. 176) and is isotypic to phenakite Be_2SiO_4.[42] γ-Si_3N_4 crystallizes in $Fd\bar{3}m$ (no. 227) in the spinel structure.[1,2] Si occupies half of the octahedral voids and one eighth of the tetrahedral voids in the cubic close packing of N atoms. Our results of the zero-pressure optimization of the crystal structures for both β- and γ-Si_3N_4 are in agreement with previous calculations (for further details, see the Supporting Information).[1,43]

$CaSiN_2$ crystallizes in the orthorhombic space group *Pbca* (no. 61).[44] The structure is built up by all side corner-sharing SiN_4 tetrahedra, to form a three-dimensional network related to the β-cristobalite structure (D1-type distortion of idealized filled C9 structure of β-cristobalite).[45] The Ca^{2+} ions are six- and eightfold coordinated by nitrogen, respectively. Coordinative Ca–N bonds can be divided into three distance groups: 235–250, 270–285, and 300–315 pm. ECoNs[28] have been calculated with MAPLE[29,30] to verify the coordination sphere of the Ca^{2+} ions. Structure optimizations for $CaSiN_2$ within the LDA and the GGA were performed. The calculations reproduced the unit cell parameters and the equilibrium volume (see Table 8) as well as the bond lengths quite well. No significant distortion of the structure after structure optimization was observed.

Table 8. Structure optimization of $CaSiN_2$.

	Experimental[44]	LDA	GGA
space group	*Pbca* (no. 61, orthorhombic)		
a [pm]	512.29(3)	505.61	516.32
b [pm]	1020.74(6)	1006.25	1027.50
c [pm]	1482.33(9)	1470.26	1485.69
V [10^6 pm^3]	775.13(8)	748.07	788.19
V f.u. [10^6 pm^3]	96.90	93.51	98.52
ρ [g cm^{-1}]	1.65	1.71	1.62

For $CaSiN_2$ we also considered a possible high-pressure phase, termed β-$CaSiN_2$ and isostructural to $CaGeN_2$[46] (B1-type distortion of the idealized filled C9 structure of β-cristobalite), which is closely related to the chalcopyrite structure.[47] It crystallizes in the tetragonal space group $I\bar{4}2d$ (no. 122). The Si atoms are tetrahedrally coordinated by N, and the Ca^{2+} ions exhibit a 4+4 bisdisphenoidal coordination. The resulting cell parameters and the obtained equilibrium volumes for the hypothetical β-$CaSiN_2$ are given in Table 9 (for bond lengths, see the Supporting Information).

Ca_3N_2 crystallizes in the anti-bixbyite structure in the body-centered space group $Ia\bar{3}$ (no. 206).[48] The N atoms are octahedrally coordinated by Ca, and the Ca atoms are fourfold coordinated by N. Our results of the zero-pressure optimization of the crystal structures for Ca_3N_2 are in agreement with previous calculations (for further details, see the Supporting Information).[49]

Table 9. Structure optimization of β-$CaSiN_2$.

	$CaGeN_2$[46]	β-$CaSiN_2$ LDA	β-$CaSiN_2$ GGA
space group	$I\bar{4}2d$ (no. 122, tetragonal)		
a [pm]	542.60	519.83	524.60
c [pm]	715.40	685.66	711.65
V [10^6 pm^3]	210.62	185.28	195.85
V f.u. [10^6 pm^3]	52.66	46.32	48.96
ρ [g cm^{-1}]	4.44	3.45	3.26

***E–V* calculations for decomposition reactions under pressure**: The phase transition of β-Si_3N_4 into γ-Si_3N_4 and the phase transition of α-$CaSiN_2$ into β-$CaSiN_2$ were taken into account for all decomposition reactions. The transition pressure for β-Si_3N_4–γ-Si_3N_4 was calculated to 11.5 GPa, and the transition pressure of α-$CaSiN_2$–β-$CaSiN_2$ to 1.6 GPa. Below these transition pressures, the enthalpy *H* for β-Si_3N_4 and α-$CaSiN_2$, respectively, was used; at higher pressures *H* for γ-Si_3N_4 and β-$CaSiN_2$ was employed.

It is found that the enthalpy of a phase agglomerate of Si_3N_4 and $2\,CaSiN_2$ is always lower than the enthalpy of a system consisting of ($2/3\,Ca_3N_2 + 5/3\,Si_3N_4$). Consequently, decomposition of $Ca_2Si_5N_8$ will result in the formation of $CaSiN_2$ and Si_3N_4 rather than Ca_3N_2 together with Si_3N_4 (see Figures 9 and 10, Tables 10 and 11).

The reaction enthalpy of the decomposition of $Ca_2Si_5N_8$ into Si_3N_4 and $CaSiN_2$ is displayed in Figure 9. Accordingly, above 15 GPa $Ca_2Si_5N_8$ will decompose into Si_3N_4 and

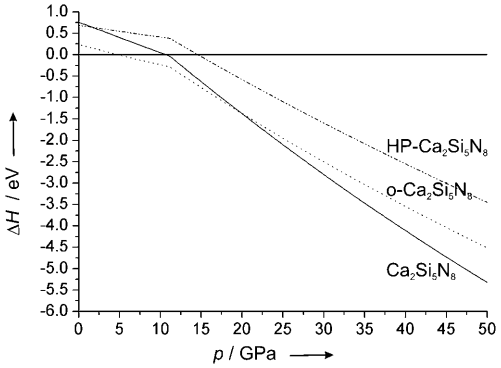

Figure 9. Enthalpy–pressure diagrams for the decomposition reactions of $Ca_2Si_5N_8$, HP-$Ca_2Si_5N_8$, and o-$Ca_2Si_5N_8$ into $CaSiN_2$ and Si_3N_4 (Murnaghan EOS evaluation).

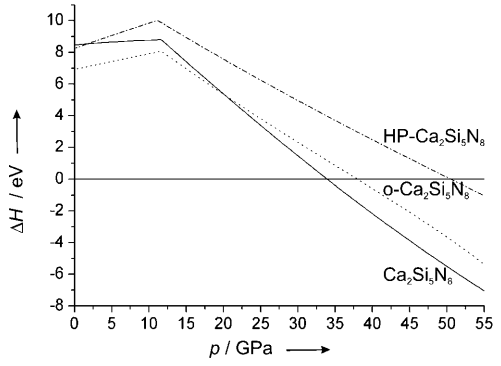

Figure 10. Enthalpy–pressure diagrams for the decomposition reactions of $Ca_2Si_5N_8$, HP-$Ca_2Si_5N_8$, and o-$Ca_2Si_5N_8$ into Ca_3N_2 and Si_3N_4 (Murnaghan EOS evaluation).

Table 10. Decomposition pressure [GPa] derived from different fitting procedures of E–V data for $Ca_2Si_5N_8$ into $CaSiN_2$ and Si_3N_4.

	$Ca_2Si_5N_8$	HP-$Ca_2Si_5N_8$	o-$Ca_2Si_5N_8$
spline	10.7	15.0	4.8
Murnaghan	10.7	14.6	4.8
Birch	10.8	14.8	4.9
Vinet	10.8	14.9	4.9
Δ_{max}	0.1	0.4	0.1

Table 11. Decomposition pressure [GPa] derived from different fitting procedures of E–V data for $Ca_2Si_5N_8$ into Ca_3N_2 and Si_3N_4.

	$Ca_2Si_5N_8$	HP-$Ca_2Si_5N_8$	o-$Ca_2Si_5N_8$
spline	33.9	50.5	38.0
Murnaghan	33.9	50.5	38.0
Birch	33.9	50.3	38.3
Vinet	34.0	50.5	38.4
Δmax	0.1	0.2	0.4

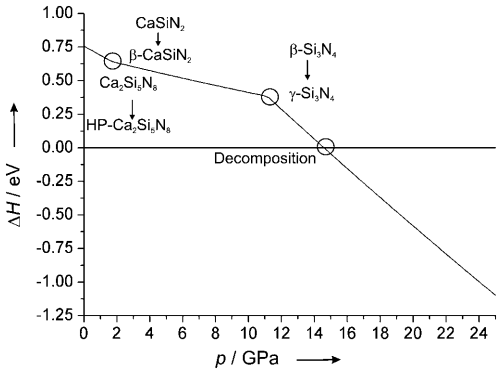

Figure 11. Enthalpy–pressure diagram for the $Ca_2Si_5N_8$–$CaSiN_2$–Si_3N_4 system (Murnaghan EOS evaluation).

Table 12. Calculated bulk moduli B_0 [GPa].

	$Ca_2Si_5N_8$		HP-$Ca_2Si_5N_8$		o-$Ca_2Si_5N_8$	
	LDA	GGA	LDA	GGA	LDA	GGA
B_0	175	162	158	147	146	139

$CaSiN_2$. This process is mainly driven by the favorable enthalpy of γ-Si_3N_4 at higher pressures. γ-Si_3N_4 is the only structure in this pressure range for which partially octahedral coordination of Si, which results in a higher density, is achieved. The possibility to further densify the matter at high pressure hence causes the decomposition of the ternary compound $Ca_2Si_5N_8$ into binary Si_3N_4 and $CaSiN_2$.

Conclusions

With the synthesis of the new high-pressure phase HP-$Ca_2Si_5N_8$, we have demonstrated that denser ternary nitridosilicates are accessible through high-pressure experiments. The HP-$Ca_2Si_5N_8$ structure consists of a centrosymmetric highly condensed network of SiN_4 tetrahedra, with $N^{[2]}$ and $N^{[3]}$ bridging. Ca^{2+} ions are enclosed in the three-dimensional nitridosilicate network, with coordination numbers of 6+1 and 7+1. Even though the structures of the ambient-pressure $Ca_2Si_5N_8$ and HP-$Ca_2Si_5N_8$ are closely related, the phase transformation is reconstructive and takes place at quite low temperatures and pressures (900 °C and 6 GPa).

Density functional calculations predicted the transition pressure of $Ca_2Si_5N_8$ into HP-$Ca_2Si_5N_8$ quite well. Monoclinic $Ca_2Si_5N_8$ is favored up to 1.7 GPa when HP-$Ca_2Si_5N_8$ becomes thermodynamically more stable. Above 15 GPa, a phased agglomerate of $2\,CaSiN_2 + \gamma\text{-}Si_3N_4$ becomes energetically more favorable (see Figure 11). Until now, we could only prove the phase transformation of $Ca_2Si_5N_8$ into HP-$Ca_2Si_5N_8$ occurring between 6 and 12 GPa by experiment.

The calculated bulk moduli (see Table 12) for both $Ca_2Si_5N_8$ modifications are quite similar, because the structures are closely related and the coordination numbers are similar. However, a remarkable property of HP-$Ca_2Si_5N_8$:Eu^{2+} is its narrower emission band compared to the emission bandwidth of ambient-pressure $Ca_2Si_5N_8$:Eu^{2+}.

Our further studies will be dedicated to the search for further high-pressure phases of ternary nitridosilicates. In analogy to γ-Si_3N_4, in which the coordination number of Si could be increased to 6, we hope to access $CN(Si) > 4$ by applying higher temperatures and pressures, thereby also aiming at the improved material properties that are already evident in HP-$Ca_2Si_5N_8$.

Experimental Section

Synthesis of $Ca_2Si_5N_8$: In a typical experiment Ca (1.86 mmol; dendritic pieces, purified by distillation, 99.99%, Aldrich) and silicon diimide (3.02 mmol; synthesized according to the literature[50]) were placed into a tungsten crucible under an argon atmosphere inside a glove box (Unilab, Fa. MBraun, Garching, $O_2 < 1$ ppm, $H_2O < 1$ ppm). Subsequently, the crucible was heated inductively in the reactor of a radio-frequency furnace[17,18] under a N_2 atmosphere (dried over silica gel/KOH/molecular sieve (pore width 4 Å)/P_2O_5 and activated BTS catalyst) to 1650 °C at a rate of 6.9 °C min^{-1} and then kept at this temperature for 1 h. Subsequently, the reaction product was cooled to 1200 °C at a rate of about 0.75 °C min^{-1} and then quenched to room temperature by switching off the furnace. A colorless, coarsely crystalline product was obtained, which according to the X-ray powder pattern was single-phase $Ca_2Si_5N_8$.

Synthesis of HP-$Ca_2Si_5N_8$: The high-pressure synthesis of HP-$Ca_2Si_5N_8$ was carried out by using the multianvil technique[19–21] with a hydraulic press. Cr_2O_3-doped MgO octahedra (Ceramic Substrates & Components Ltd., Isle of Wight, UK) with an edge length of 14 mm were used. Eight truncated tungsten carbide cubes separated by pyrophyllite gaskets served as anvils for the compression of the octahedra. The truncation edge length was 8 mm. Powder of ambient-pressure $Ca_2Si_5N_8$ was loaded into a cylindrical capsule of hexagonal boron nitride (Henze, Kempten) with a capacity of 9 mm^3 and sealed with a BN cap. The capsule was centered within two nested graphite tubes, which acted as an electrical resistance furnace. The remaining volume at both ends of the sample capsule was filled with two cylindrical pieces of magnesium oxide. The arrangement was placed into a zirconium dioxide tube and then transferred into a pierced MgO octahedron. The electrical contact of the graphite tubes was arranged by two plates of molybdenum. The assembly was compressed up to 8 GPa at room temperature within 2.5 h and then heated to

1000 °C within 12 min. The sample was treated for 12 min under these conditions and then cooled to 600 °C within 30 min. After that the sample was quenched to room temperature, followed by decompression for 7.5 h. By this procedure about 5 mg of HP-$Ca_2Si_5N_8$ was obtained as a dark gray substance. The temperature was calculated from the electrical power applied to the furnace, which was determined on the basis of calibration curves from measurements with $W_{97}Re_3W_{75}Re_{25}$ thermocouples, as described in reference [51].

Single-crystal X-ray diffraction: Small single crystals of HP-$Ca_2Si_5N_8$ were isolated by mechanical fragmentation and checked by Laue photographs. Single-crystal X-ray data were collected on a Stoe IPDS diffractometer ($Mo_{K\alpha}$ radiation). The program SHELXD[22] was used for solution of the structure and SHELXL97 for refinement. Further details of the crystal structure investigations can be obtained from the Fachinformationszentrum Karlsruhe, 76344 Eggenstein-Leopoldshafen, Germany (fax: (+49) 7247-808-666; E-mail: crysdata@fiz-karlsruhe.de) on quoting the depository number CSD-419318.

Powder X-ray diffraction: X-ray diffraction experiments on powder samples of HP-$Ca_2Si_5N_8$ were performed on a Stoe Stadi P powder diffractometer in Debye–Scherrer geometry, with Ge(111)-monochromatized $Cu_{K\alpha1}$ radiation ($\lambda = 154.056$ pm). The microcrystalline sample was enclosed in a glass capillary of diameter 0.1 mm. A Rietveld refinement was carried out by using the program package GSAS.[52] The atomic parameters of the single-crystal structure of HP-$Ca_2Si_5N_8$ were used as starting values and were refined together with the isotropic displacement factors. β-Si_3N_4[43] was present in the powder diffraction pattern as a minor impurity and was refined as a second phase. (The observed and calculated X-ray powder diffraction patterns and difference profile of the Rietveld refinement are shown in Figure 1.) Further details on the refinement are given in Table 13. The refined atomic coordinates do not differ by more than 0.0075 pm from those obtained from single-crystal data. Ca–N distances range from 239.11 to 300.78 pm and Si–N distances from 166.01 to 182.74 pm, and differ only by a maximum of 5.23 pm for Ca–N and 2.39 pm for Si–N relative to the distance ranges obtained from single-crystal data.

Table 13. Crystallographic data of HP-$Ca_2Si_5N_8$ derived from Rietveld refinement.

formula	$Ca_2Si_5N_8$
formula mass [g mol^{-1}]	332.65
crystal system	orthorhombic
space group	*Pbca* (no. 61)
cell parameters [pm]	$a = 1057.11(2)$
	$b = 963.81(2)$
	$c = 1362.50(2)$
cell volume [10^6 pm^3]	1388.19(4)
formula units/cell	8
X-ray density [g cm^{-3}]	3.18
$F(000)$	1328
diffractometer	Stoe Stadi P
radiation [pm]	$Cu_{K\alpha1}$ ($\lambda = 154.056$ pm)
monochromator	Ge(111)
temperature [K]	293
profile range (2θ) [°]	$5 \le 2\theta \le 89.89$
no. of data points	8489
hkl	$0 \le h \le 9$, $0 \le k \le 8$, $0 \le l \le 12$
observed reflections	611
no. of refined parameters:	
atomic parameters	58
profile parameters	12 (6 each phase)
other parameters	3
structure refinement	Rietveld refinement, GSAS[52]
background function	shifted Chebyschev
profile function	pseudo-Voigt
R_p	0.0289
wR_p	0.0382
$R_{\lvert F\rvert^2}$	0.07644
GOF	1.11
reduced χ^2	1.222

Luminescence: Photoluminescence measurements were carried out with a spectrofluorimeter equipped with a 150 W Xe lamp, two 500 mm Czerny–Turner monochromators, 1800 1/mm lattices, and 250/500 nm lamps, with a spectral range from 230 to 820 nm.

EDX measurements: The carbon-coated sample was examined with a scanning electron microscope (JSM-6500F, Joel, Japan; maximum acceleration voltage 30 kV). An energy-dispersive spectrometer Model 7418 (Oxford Instruments, UK) allowed qualitative and semiquantitative elemental analysis.

Raman measurements: Raman spectra were recorded on a Jobin Yvon Horiba HR800 UV/Raman microscope with a He–Ne laser emitting at 632.8 nm (for further details, see the Supporting Information).

Computational methods: The total energies and atomic structures of all materials were calculated within DFT.[53] The Vienna ab initio simulation package (VASP) was used, which combines the total-energy pseudopotential method with a plane-wave basis set.[54–56] The LDA[57,58] and GGA[59] were used to approximate the electron exchange and correlation energy. The pseudopotentials taken were based on the projector-augmented-wave (PAW) method.[60] The cutoff energy for the expansion of the wave function into the plane-wave basis set was 500 eV. Residual forces were converged below 5×10^{-3} eV Å^{-1}. The Brillouin-zone integration was carried out by the Monkhorst–Pack scheme.[61]

Structure optimizations were performed by relaxing all internal parameters as well as cell parameters and the unit cell volume. The unit cell of $Ca_2Si_5N_8$ contains 60 atoms. By transforming it into a primitive unit cell, this could be reduced to 30 atoms per cell, which corresponds to two formula units. A *k*-point mesh of $3 \times 3 \times 2$ was used. The unit cell of HP-$Ca_2Si_5N_8$ contains 120 atoms. This unit cell is already the primitive cell, and contains eight formula units. A *k*-point mesh of $2 \times 2 \times 2$ was used. The unit cell of o-$Ca_2Si_5N_8$ contains 30 atoms, which corresponds to two formula units, and is already a primitive cell. A *k*-point mesh of $4 \times 4 \times 2$ was used. The unit cell of β-Si_3N_4 contains 14 atoms and is already a primitive cell that contains two formula units. A *k*-point mesh of $3 \times 3 \times 8$ was used. The unit cell of γ-Si_3N_4 contains 56 atoms. By transforming it into a primitive unit cell, this could be reduced to 14 atoms, which corresponds to two formula units. A *k*-point mesh of $4 \times 4 \times 4$ was used. The unit cell of $CaSiN_2$ contains 64 atoms (16 formula units). Calculations were carried out in the conventional cell. A *k*-point mesh of $4 \times 2 \times 2$ was used. The unit cell of Ca_3N_2 contains 80 atoms (16 formula units). Calculations were performed in the conventional unit cell. A k-point mesh of $2 \times 2 \times 2$ was used.

To obtain the bulk modulus the volume was varied around the zero-pressure volume V_0 and the calculated energies were fitted to Murnaghan's, Birch's, and Vinet's equations of state (EOS).[62–64]

The *E*–*V* diagrams can be transformed easily to give enthalpy versus pressure diagrams. To obtain the pressure *p* from the *E*–*V* graph, a simple numerical differentiation of a spline fit and Murnaghan's, Birch's, and Vinet's EOS was employed: $p = -\partial E/\partial V$. Evaluation of the *E*–*V* data by fitting to a spline fit or different EOS resulted in virtually the same transition pressures. The largest difference observed was 0.4 GPa in the p_t for $Ca_2Si_5N_8$ into o-$Ca_2Si_5N_8$ and 0.5 GPa for the decomposition pressure of o-$Ca_2Si_5N_8$ into Ca_3N_2 and Si_3N_4 (see Tables 7, 10, and 11).

For reasons of simplicity, all figures and values given in this work are derived from evaluation by Murnaghan's EOS (see Tables 7, 10, and 11 for details). The enthalpy *H* was calculated by $H = E + pV$. In equilibrium a system will adopt the structure with the lowest free energy *G*. A phase transformation is therefore governed by the difference in free enthalpy: $\Delta G = \Delta E + p\Delta V - T\Delta S$. The contribution of the entropy is usually neglected, due to the small difference in entropy between solid-state crystal structures and the comparably larger changes of ΔH within 1 GPa of pressure change. Therefore, $\Delta H = \Delta E + p\Delta V$ is a good measure to compare the relative stability of solid-state structures under pressure.

Acknowledgements

Financial support by the Deutsche Forschungsgemeinschaft (priority program SPP 1236, project SCHN 377/13 and Kr 1805/10 and Heisenberg program Kr 1805/9) and the Fonds der Chemischen Industrie (FCI), Germany, is gratefully acknowledged. We would also like to thank Christian Schmolke (LMU München) for the first synthesis of HP-$Ca_2Si_5N_8$, Dr. Atsushi Togo (RWTH Aachen) for calculating the phonon band structures of o-$Ca_2Si_5N_8$, Christian Minke (LMU München) for the EDX measurements, and Johann Kecht (LMU München) for the Raman measurements. Furthermore, we would like to thank the Leibniz Rechenzentrum, Munich, for computational resources on the Linux Cluster System and the Höchstleistungsrechner in Bayern, HLRB II, as well as the Texas Advanced Computing Center at Austin.

[1] A. Zerr, G. Miehe, G. Serghiou, M. Schwarz, E. Kroke, R. Riedel, H. Fueß, P. Kroll, R. Boehler, *Nature* **1999**, *400*, 340–342.
[2] M. Schwarz, G. Miehe, A. Zerr, E. Kroke, B. T. Poe, H. Fuess, R. Riedel, *Adv. Mater.* **2000**, *12*, 883–887.
[3] W. Schnick, *Int. J. Inorg. Mater.* **2001**, *3*, 1267–1272.
[4] T. Schlieper, W. Milius, W. Schnick, *Z. Anorg. Allg. Chem.* **1995**, *621*, 1380–1384.
[5] H. Huppertz, W. Schnick, *Acta Crystallogr. Sect. C* **1997**, *53*, 1751–1753.
[6] S. Hampshire in *Materials Science and Technology, Vol. 11* (Eds.: R. W. Cahn, P. Haasen, E. J. Kramer), Wiley-VCH, Weinheim, **1994**.
[7] L.-O. Nordberg, M. Nygren, P.-O. Käll, Z. Shen, *J. Am. Ceram. Soc.* **1998**, *81*, 1461–1470.
[8] R. Mueller-Mach, G. Mueller, M. R. Krames, H. A. Höppe, F. Stadler, W. Schnick, T. Juestel, P. Schmidt, *Phys. Status Solidi A* **2005**, *202*, 1727–1732.
[9] T. Jüstel, H. Nikol, C. Ronda, *Angew. Chem.* **1998**, *110*, 3250–3271; *Angew. Chem. Int. Ed.* **1998**, *37*, 3084–3103.
[10] C. Ronda, *Luminescence: From Theory to Applications*, Wiley-VCH, Weinheim, **2008**.
[11] H. A. Höppe, H. Lutz, P. Morys, W. Schnick, A. Seilmeier, *J. Phys. Chem. Solids* **2000**, *61*, 2001–2006.
[12] L. W. Finger, R. M. Hazen, *Rev. Mineral. Geochem.* **2001**, *41*, 123–155.
[13] R. M. Hazen, R. T. Downs, L. W. Finger, *Science* **1996**, *272*, 1769–1771.
[14] N. Dubrovinskaia, L. S. Dubrovinsky, *Mater. Chem. Phys.* **2001**, *68*, 77–79.
[15] J. M. Leger, J. Haines, M. Schmidt, J. P. Petitet, A. S. Pereira, J. A. H. da Jornada, *Nature* **1996**, *383*, 401.
[16] W. Schnick, *Angew. Chem.* **1993**, *105*, 846–858; *Angew. Chem. Int. Ed. Engl.* **1993**, *32*, 806–818.
[17] W. Schnick, H. Huppertz, R. Lauterbach, *J. Mater. Chem.* **1999**, *9*, 289–296.
[18] T. Schlieper, W. Schnick, *Z. Anorg. Allg. Chem.* **1995**, *621*, 1037–1041.
[19] H. Huppertz, *Z. Kristallogr.* **2004**, *219*, 330–338.
[20] D. Walker, M. A. Carpenter, C. M. Hitch, *Am. Mineral.* **1990**, *75*, 1020–1028.
[21] D. Walker, *Am. Mineral.* **1991**, *76*, 1092–1100.
[22] G. M. Sheldrick, SHELXD, program for the solution of crystal structures, University of Göttingen, Germany, **2002**.
[23] The term "*dreier* ring" was coined by Liebau and is derived from the German word "drei", which means three; however, a *dreier* ring is not a three-membered ring, but a six-membered ring comprising three tetrahedral centers (Si) and three electronegative atoms (N). Similar terms exist for rings comprising four, five, and six tetrahedral centers (and the corresponding number of electronegative atoms), namely *vierer*, *fünfer*, and *sechser* rings, respectively. (F. Liebau, *Structural Chemistry of Silicates*, Springer, Berlin, **1985**.).
[24] W. E. Klee, *Z. Kristallogr.* **1987**, *179*, 67–76.
[25] A. Beukemann, W. E. Klee, *Z. Kristallogr.* **1992**, *201*, 37–51.
[26] A. Beukemann, W. E. Klee, *Z. Kristallogr.* **1994**, *209*, 709–713.
[27] G. Thimm, S. Schumacher, W. Uhr, W. E. Klee, TOPOLAN, program for topological analysis of crystal structures, University of Karlsruhe, Germany, **1993**.
[28] R. Hoppe, *Angew. Chem.* **1970**, *82*, 7–16; *Angew. Chem. Int. Ed. Engl.* **1970**, *9*, 25–34.
[29] a) R. Hoppe, *Angew. Chem.* **1966**, *78*, 52–63; *Angew. Chem. Int. Ed. Engl.* **1966**, *5*, 95–106; b) R. Hoppe, *Z. Naturforsch. A* **1995**, *50*, 555–567; c) C. Weiß, R. Hoppe, *Z. Anorg. Allg. Chem.* **1996**, *622*, 1019–1026.
[30] R. Hübenthal, MAPLE Vers. 4, University of Gießen, **1993**.
[31] I. D. Brown, D. Altermatt, *Acta Crystallogr. Sect. B* **1985**, *41*, 244–247.
[32] N. E. Brese, M. O'Keeffe, *Acta Crystallogr. Sect. B* **1991**, *47*, 192–197.
[33] R. Hoppe, S. Voigt, H. Glaum, J. Kissel, H. P. Muller, K. J. Bernet, *J. Less-Common Met.* **1989**, *156*, 105–122.
[34] I. Idrestedt, C. Brosset, *Nature* **1964**, *201*, 1211–1211.
[35] R.-J. Xie, N. Hirosaki, T. Suehiro, F.-F. Xu, M. Mitomo, *Chem. Mater.* **2006**, *18*, 5578–5583.
[36] K. Uheda, N. Hirosaki, H. Yamamoto, *Phys. Status Solidi A* **2006**, *203*, 2712–2717.
[37] P. Schmidt, A. Tuecks, J. Meyer, H. Bechtel, D. Wiechert, R. Mueller-Mach, G. Mueller, W. Schnick, Philips Research Europe, Aachen, Germany. Proceedings of SPIE—The International Society for Optical Engineering, Seventh International Conference on Solid-State Lighting, **2007**, 66690P/1–66690P/9.
[38] Fang et al. calculated the electronic structure of $Ca_2Si_5N_8$, but did not give the calculated cell parameters. Therefore, no comparison with their results was possible. (C. M. Fang, H. T. Hintzen, G. de With, R. A. de Groot, *J. Phys. Condens. Matter* **2001**, *13*, 67–76.).
[39] R. D. Shannon, *Acta Crystallogr. Sect. A* **1976**, *32*, 751–767.
[40] W. H. Baur, *Crystallogr. Rev.* **1987**, *1*, 59–83.
[41] In our calculations, LDA even favors HP-$Ca_2Si_5N_8$ over the ambient-pressure modification $Ca_2Si_5N_8$. This phenomenon of LDA greatly underestimating transition pressures is not unknown. Demuth et al. showed that for SiO_2, LDA underestimates the transition pressure of α-quartz into coesite by 59% and the transition pressure of coesite into stishovite by 78%.(Th. Demuth, Y. Jeanvoine, J. Hafner, J. G. Ángyán, *J. Phys. Condens. Matter* **1999**, *11*, 3833–3874.).
[42] D. Hardie, K. H. Jack, *Nature* **1957**, *180*, 332–333.
[43] P. Kroll, M. Milko, *Z. Anorg. Allg. Chem.* **2003**, *629*, 1737–1750.
[44] Z. A. Gál, P. M. Mallinson, H. J. Orchard, S. J. Clarke, *Inorg. Chem.* **2004**, *43*, 3998–4006.
[45] J. G. Thompson, R. L. Withers, S. R. Palethorpe, A. Melnitchenko, *J. Solid State Chem.* **1998**, *141*, 29–49.
[46] M. Maunaye, J. Guyader, Y. Laurent, J. Lang, *Bull. Soc. Fr. Mineral. Cristallogr.* **1971**, *94*, 347–352.
[47] S. R. Römer, P. Kroll, W. Schnick, unpublished results.
[48] Y. Laurent, J. Lang, M. Th. LeBihan, *Acta Crystallogr. Sect. B* **1968**, *24*, 494–499.
[49] E. Orhan, S. Jobic, R. Brec, R. Marchand, J.-Y. Saillard, *J. Mater. Chem.* **2002**, *12*, 2475–2479.
[50] F. Stadler, PhD thesis, Ludwig-Maximilians-Universität München (Germany), **2006**.
[51] D. C. Rubie, *Phase Transitions* **1999**, *68*, 431–451.
[52] A. C. Larson, R. B. von Dreele, *GSAS—Generalized Structure Analysis System*, Los Alamos National Laboratory, Los Alamos, NM, USA, LAUR **2004**, pp. 86–748.
[53] P. Hohenberg, W. Kohn, *Phys. Rev. B* **1964**, *136*, 864–871.
[54] a) G. Kresse, J. Hafner, *Phys. Rev. B* **1993**, *47*, 558–561; b) G. Kresse, J. Hafner, *Phys. Rev. B* **1994**, *49*, 14251–14269.
[55] G. Kresse, J. Furthmüller, *Comput. Mater. Sci.* **1996**, *6*, 15–50.
[56] G. Kresse, J. Furthmüller, *Phys. Rev. B* **1996**, *54*, 11169–11186.
[57] J. P. Perdew, A. Zunger, *Phys. Rev. B* **1981**, *23*, 5048–5079.
[58] D. M. Ceperley, B. J. Alder, *Phys. Rev. Lett.* **1980**, *45*, 566–569.
[59] J. P. Perdew in *Electronic Structures of Solids '91* (Eds.: P. Ziesche, H. Eschrig), Akademie, Berlin, **1991**.
[60] G. Kresse, J. Joubert, *Phys. Rev. B* **1999**, *59*, 1758–1775.

[61] H. J. Monkhorst, J. D. Pack, *Phys. Rev. B* **1976**, *13*, 5188–5192.
[62] F. D. Murnaghan, *Proc. Natl. Acad. Sci. USA* **1944**, *30*, 244–247.
[63] F. Birch, *J. Geophys. Res.* **1952**, *57*, 227–286.
[64] a) P. Vinet, J. Ferrante, J. R. Smith, J. H. Rose, *Phys. Rev. B* **1987**, *35*, 1945–1953; b) P. Vinet, J. H. Rose, J. Ferrante, J. R. Smith, *J. Phys. Condens. Matter* **1989**, *1*, 1941–1963.

Received: April 1, 2008
Published online: July 15, 2008

